USGS
science for a changing world

**Prepared for the National Aeronautics and Space Administration**

# Geologic Map of MTM –10022 and –15022 Quadrangles, Morava Valles and Margaritifer basin, Mars

By Sharon A. Wilson, John A. Grant, and Kevin K. Williams

Pamphlet to accompany
Scientific Investigations Map 3489

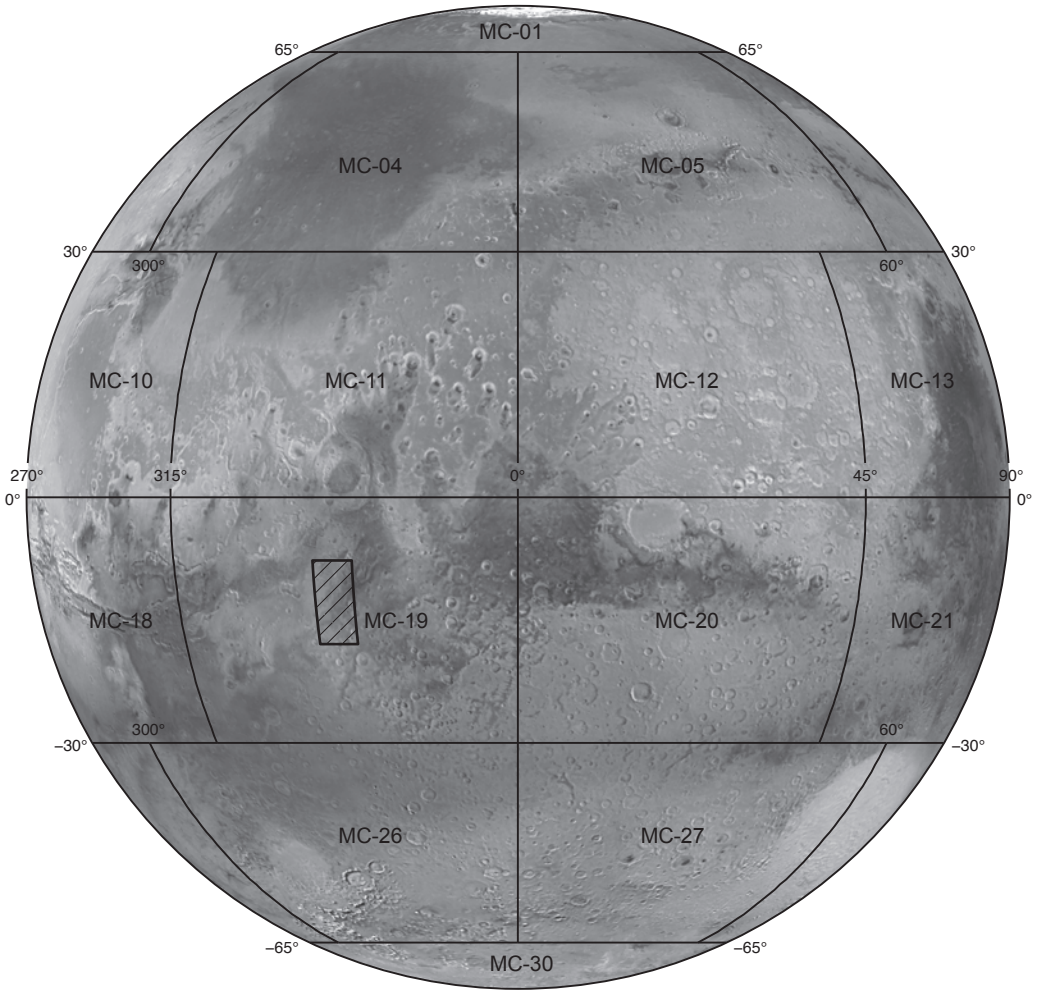


2022

**U.S. Department of the Interior**
**U.S. Geological Survey**

U.S. Geological Survey, Reston, Virginia: 2022



Suggested citation:
Wilson, S.A., Grant, J.A., and Williams, K.K., 2022, Geologic map of MTM –10022 and –15022 quadrangles, Morava Valles and Margaritifer basin, Mars: U.S. Geological Survey Scientific Investigations Map 3489, pamphlet 11 p., 1 sheet, scale 1:500,000, https://doi.org/10.3133/sim3489.

ISSN 2329-1311 (print)
ISSN 2329-132X (online)

**Cover.** Photomosaic showing location of map area (hachured rectangle). An outline of 1:5,000,000-scale quadrangles is provided for reference.

# Contents

Introduction and Background....1
Mapping Methods and Data....2
Age Determinations....3
Regional Geology....3
Stratigraphy....4
Noachian Period....4
Hesperian Period....4
Amazonian Period....6
Structural Features....7
Geologic Summary....7
Acknowledgements....8
References Cited....8

## Figures

1. Topographic map of Margaritifer Terra region of Mars showing locations of regional landforms and drainage systems....map sheet
2. Topographic map showing Mars Transverse Mercator –10022 and –15022 quadrangles....map sheet
3. Graphs showing cumulative crater statistics for units defined in Mars Transverse Mercator –10022 and –15022 quadrangles....map sheet
4. Context Camera (CTX) image showing Samara-Himera Valles in Mars Transverse Mercator –15022 quadrangle....map sheet
5. Context Camera (CTX) images showing contact relations of basin fill 2 unit ($HNb_2$). *A*, Local occurrences of valley networks (unit HNvn) near lat –16.1° N., long 337.3° E. buried by basin fill 2 unit ($HNb_2$). *B*, The smooth, less cratered, unit HNb2 embays the rough, cratered unit HNt unit....map sheet
6. Topographic map showing that early discharge through Morava Valles (unit $HNch_1$) carved channels in the terra unit (HNt) that are more degraded and ~200–300 meters shallower relative to the smooth floors that formed during later discharge events....map sheet
7. Image showing that the floor of Morava Valles (unit $AHch_2$) incised into a remnant of the basin fill 3 unit ($Hb_3$) and created a series of terraces, which cut into the terra unit (HNt) bedrock....map sheet
8. Image showing approximate contact between light-toned, scabby basin fill 1 unit ($HNb_1$) that underlies smoother basin fill 3 unit ($Hb_3$) in Margaritifer basin....map sheet
9. Cross section (*A*) and topographic map (*B*) showing Samara-Himera and Loire valley systems and part of the Margaritifer basin....map sheet

## Table

1. Characteristics used to estimate absolute age and associated epoch of geologic units in the map region....3

# Geologic Map of MTM –10022 and –15022 Quadrangles, Morava Valles and Margaritifer Basin, Mars

By Sharon A. Wilson[1], John A. Grant[1], and Kevin K. Williams[2]

## Introduction and Background

The Late Noachian to Hesperian landscape and stratigraphy on Mars records an important chapter in the aqueous history of the planet because the climate during this time favored widespread valley formation and, at least sometimes, sustained an active hydrologic cycle (for example, Grant, 2000; Grant and Parker, 2002; Howard and others, 2005; Carr, 2006; Fassett and Head, 2008; Grant and others, 2009). Evaluating the drainage evolution over this period, as it relates to possible past habitable conditions that occurred near the end of this early, wetter period on Mars (Bibring and others, 2005), provides insight into the timing of the transition to colder and drier present-day conditions.

Prior geologic and geomorphic maps of the Margaritifer Terra region (Saunders, 1979; Grant, 1987, 2000; Rotto and Tanaka, 1995; Grant and Parker, 2002; Irwin and Grant, 2013; Tanaka and others, 2014; Salvatore and others, 2016) constrain the general timing of activity along a segmented, mesoscale outflow system, consisting of Uzboi Vallis, Ladon Valles, and Morava Valles, with respect to other regional geomorphic events (Saunders, 1979; Scott and Tanaka, 1986; Parker, 1985, 1994; Grant, 1987, 2000; Grant and Parker, 2002; Pondrelli and others, 2005; Grant and others, 2008, 2009; Wilson and others, 2018). The northward-draining Uzboi-Ladon-Morava (ULM) mesoscale outflow system was sourced from flow out of Argyre basin and incises across and between the ancient Ladon and Holden impact basins (fig. 1) (Grant and Parker, 2002; Grant and others, 2008; 2010; Irwin and Grant, 2013). The system terminates in a broad, southwest-northeast-elongated depression informally named Margaritifer basin, which formed along the axis of a linear depression known as the "Chryse trough" (Saunders, 1979; Phillips and others, 2001). Margaritifer basin is the catchment for Morava Valles, the lowermost reach of the ULM system and the drainage outlet from Ladon basin (fig. 1). Margaritifer Chaos bounds the northeast and northwest edges of Margaritifer basin, and the collapse associated with its formation disrupts the surface and complicates interpretation of possible connections between the ULM mesoscale outflow system and the northern plains via Ares Vallis (Rotto and Tanaka, 1995; Grant and Parker, 2002) and (or) Mawrth Vallis (Irwin and Grant, 2009).

The ULM mesoscale outflow system drains nearly 9 percent of the Martian surface, or more than $11 \times 10^6$ square kilometers ($km^2$) (Phillips and others, 2001; Grant and Parker, 2002). Incision of the ULM system likely occurred during multiple large discharge events (Grant and Parker, 2002; Irwin and Grant, 2013), as supported by the anabranching outlet valleys, that likely resulted from filling and overflowing of the large intervening basins from discharges so large that the pre-valley topography could not confine the flow(s) into a single channel. The hanging relationship between side channels and the main stem indicates that multiple overflow points remained active until the central channel was incised deeply enough to confine the entire flow. This is consistent with possible terraces along Uzboi Vallis (Wilson and others, 2018) and at least five distinct terraces along Ladon Valles (Boothroyd, 1982; Parker, 1985; Grant, 1987; Grant and Parker, 2002). Discharge estimates during incision of the ULM system are uncertain, but the elevation of terraces along Ladon Valles, combined with channel cross-section dimensions and gradient, indicate discharge rates between 150,000 and 450,000 cubic meters per second (Grant and Parker, 2002). Such rates are 5–10 times higher than that of the Mississippi River (Komar, 1979) and on the lower end of discharge rates from the Channeled Scablands (Baker and Nummedal, 1978; Baker, 1982).

The Samara-Himera and Paraná-Loire valley network systems dominate drainage southeast of Margaritifer basin (fig. 1). The confluence of the Samara-Himera and Paraná-Loire valley systems is located south of Margaritifer basin (Williams and others, 2005) in Mars Transverse Mercator (MTM) −15022 quadrangle, but the connection of the valleys to the basin is largely obscured by younger volcanic deposits and locally collapsed surfaces. The Samara-Himera and Paraná-Loire valley systems form two of the most laterally extensive, well-integrated valley networks on the planet (Grant, 2000) that drain approximately 540,000 $km^2$, equivalent to ~85 percent of the Colorado River watershed on Earth. These valley network systems also contribute to one of the highest preserved density of drainage networks on Mars (Carr, 1981, 1996; Baker, 1982), consistent with a paleoclimate that supported fluvial processes (Carr, 1981, 1996, 2006; Mars Channel Working Group, 1983; Baker and others, 1992;

[1]Smithsonian Institution

[2]State University of New York at Buffalo

Grant, 2000; Grant and Parker, 2002). Nevertheless, the degraded appearance of the valleys limits confident definition of an incised channel, precluding meaningful discharge estimates.

Numerous non-crater-related geologic units from previous investigations have been mapped and described within MTM −10022 and −15022 quadrangles. On a global scale (1:20,000,000), geologic mapping by Tanaka and others (2014) identified three main units: Middle Noachian highlands (mNh), Noachian highland undivided (Nhu), and Hesperian transition (Ht). At the quadrangle scale (1:5,000,000), Saunders (1979) identified cratered plateau material (pc), chaotic material (cht), and channel deposits (chs). Rotto and Tanaka (1995), at a scale of 1:5,000,000, further divided the highland plateau and high plains into hilly (Nplh), dissected (Npld), cratered ($Npl_1$), subdued cratered ($Npl_2$), older ridged plains (HNr), and undivided (Hnu) units. They also mapped chaotic terrain (Hctl, Hcth) and channel (Hchh) units. The prominent units in the geologic/geomorphic map by Grant (1987) at a scale of 1:2,000,000 are heavily cratered terrain (Hc), undifferentiated smooth plains (Spu), chaotic terrain (Ctm and Ctet), and channels and valleys (Ch). Several units mapped in the adjacent, contemporary map to the west at 1:1,000,000 scale by Irwin and Grant (2013) were also identified in MTM −10022 and −15022 quadrangles, including plateau and highland units (HNt, Nm), channel fill units ($HNch_1$), basin fill units ($HNb_1$, $HNb_2$, $Hb_3$), and severely deformed/chaotic units (AHct). Salvatore and others (2016) identified compositionally, thermophysically, and morphologically distinct geologic units within Margaritifer basin including a mountainous unit (MU), fractured unit (FRU), channel fill unit (CFU), flat lying plains unit (FLPU), and chaotic terrain. In our geologic map, units HNt, $Hb_3$, $AHch_2$, and $HNb_1$ broadly correlate to Salvatore and others (2016) units MU, FLPU, CFU, and FRU, respectively.

Despite prior mapping in the region, important questions related to the ULM and the evolution of Margaritifer basin remain. For example, relative discharge contributions to Margaritifer basin from the ULM versus the Samara-Himera and Parana-Ladon valley system are unknown. In addition, whether the ULM was through-flowing into Margaritifer basin during multiple discharge events or a single discharge event has implications for the storage of water within Margaritifer basin and (or) upstream within Ladon basin. Moreover, any connection between water reaching Margaritifer basin and discharges farther to the north via Ares and (or) Mawrth Valles (outside of map area) was uncertain. Information related to each of these questions has implications for the source and duration of water over a broad part of the Martian surface and the occurrence of associated habitable conditions on the planet. Herein, we provide a new geological and geomorphic map at 1:500,000 scale in MTM −10022 and −15022 quadrangles (lat −7.5° N. to −17.5° N. between long 335° E. and 340° E.) (fig. 1). This map builds on prior mapping and fills a gap between existing maps to refine the history of fluvial incisement and resurfacing in the region by a variety of processes. This map helps to constrain the timing, relative contributions, and fate of water that debouched into Margaritifer basin. Because the basin lies at the confluence of mesoscale outflow drainages as well as the best preserved and integrated valley systems on Mars, unraveling its history has broader implications for the timing and sources of water on Mars at a global scale.

# Mapping Methods and Data

We used basic planetary mapping principles (for example, Mutch and others, 1976; Greeley and Batson, 1990; Ford and others, 1993; Tanaka and others, 1994) to define map units based on topography, morphology, stratigraphic relations, and relative age. During mapping, we used methods and formats consistent with current established guidelines and protocols described by Tanaka and others (2011) and Skinner and others (2018). Where unique primary morphology was evident, we designated unit names that were descriptive (for example, fan unit, chaotic unit, volcanic unit). For units with more ambiguous origins and (or) compositions, we assigned unit names on the basis of their geographic and stratigraphic locations (for example, basin fill 1 unit is older than basin fill 3 unit, see table 1) after Irwin and Grant (2013).

Regional context for mapping was provided by previous mapping at smaller scales (Saunders, 1979; Scott and Tanaka, 1986; Greeley and Guest, 1987; Tanaka and others, 2014) and at comparable scales elsewhere in Margaritifer Terra (Grant and others, 2009; Irwin and Grant, 2013). These maps enabled initial definition of some of the units in MTM −10022 and −15022 quadrangles, and other units were described by Grant (1987) in association with drainage basin mapping. We consulted adjacent maps to the west, detailing the geology of Holden crater and eastern Ladon basin at 1:1,000,000 scale (Irwin and Grant, 2013), to ensure unit definitions were consistent across both maps. We defined additional units, described herein, as a result of mapping with higher resolution and diverse data at a map scale of 1:500,000. Geomorphic units in the map area are varied in their expression and reflect a history of diverse geologic processes. As with all photogeologic mapping, however, origin of some units may have multiple interpretations. In addition to the geomorphology discussed below, most units incorporate, or are overprinted, at least in part, by some amount of impact debris because of the widespread extent of cratering throughout the geologic record on Mars.

We compiled and analyzed the datasets, described below, in a geographic information system (GIS) project. We drafted line work at 1:125,000 scale for publication at 1:500,000 and used a stream-digitized vertex spacing of ~125 m. Unit contacts were attributed as certain or approximate. We mapped numerous linear features including ridge crests, graben, fluvial valleys, troughs, scarp crests, scarp bases, depressions, and crater rims.

We used the global daytime and nighttime infrared (IR) mosaics from the Thermal Emission Imaging System (THEMIS, ~100 meter per pixel [m/pixel] resolution) (Christensen and others, 2004) on the Mars Odyssey spacecraft and a mosaic of images from the Context Camera (CTX, ~5–6 m/pixel resolution) (Malin and others, 2007; Dickson and others, 2018) on board the Mars Reconnaissance Orbiter (MRO). We generated a topographic base map from gridded Mars Orbiter Laser Altimeter (MOLA) (128 pixel per degree or ~463 m/pixel resolution) (Smith and others, 2001) data, an instrument on Mars Global Surveyor (MGS) (fig. 2). All base maps used a transverse Mercator projection with a central meridian of 340° E. Horizontal coordinate information is referenced to the Mars 2000 sphere. Elevations are referenced to the MOLA defined areoid, which is an equipotential surface whose average value at the equator is 3,396.190 kilometers (km) (Smith and others, 2001).

**Table 1.** Table 1. Characteristics used to estimate absolute age and associated epoch of geologic units in the map region.

[Abbreviations: Ga, billion years ago; km, kilometer; km$^2$, square kilometer; n/a, not applicable]

| Unit name (label) | Combined unit area, in km$^2$ | Best fit crater diameter range, in km | Number of craters used in diameter range | Estimated absolute age (range), in Ga | Epoch |
|---|---|---|---|---|---|
| Chaotic 2[1] (AHct$_2$) | 14,200 | 0.8–1.5 | 10 | 1.03 (±0.27) | Middle Amazonian to Late Hesperian |
| Chaotic 1[1] (AHct$_1$) | 13,400 | 0.6–2.5 | 46 | 1.38 (±0.20) | Middle to Early Amazonian to Late Hesperian |
| Mass wasting (AHmw) | 37 | n/a | n/a | n/a | Amazonian to Hesperian (?) |
| Channel 2[2] (AHch$_2$) | 3,260 | 0.5–2.5 | 73 | 2.64 (+0.27 / −0.30) | Early Amazonian to Late Hesperian |
| Volcanic[1] (AHv) | 4,220 | 0.6–3 | 25 | 2.84 (+0.34 / −0.54) | Early Amazonian to Late Hesperian |
| Fan[1] (AHf) | 272 | 0.6–1 | 2 | 3.13 (+0.36 / −2.10) | Middle Amazonian to Late Hesperian |
| Basin fill 3[2] (Hb$_3$) | 26,400 | 1.5–14 | 17 | 3.39 (+0.05 / −0.08) | Late Hesperian |
| Basin fill 2[2] (HNb$_2$) | 4,560 | 1–12 | 105 | 3.63 (±0.02) | Late Hesperian to Early Hesperian/Late Noachian |
| Basin fill 1[2] (HNb$_1$) | 7,170 | 1–6 | 24 | 3.62 (+0.04 / −0.06) | Late Hesperian to Early Hesperian/Late Noachian |
| Channel 1[2] (HNch$_1$) | 1,320 | 0.8–2.5 | 9 | 3.54 (+0.08 / −0.16) | Late Hesperian to Early Hesperian/Late Noachian |
| Vallis (HNvn) | 1,235 | n/a | n/a | n/a | Early Hesperian to Late Noachian |
| Terra[1] (HNt) | 65,600 | 4.5–60 | 29 | 3.84 (±0.03) | Early Hesperian to Late Noachian |
| Mountainous (Nm) | 632 | n/a | n/a | n/a | Middle Noachian (Schultz and others, 1982) |

[1]Cumulative plot on figure 3*A*.

[2]Cumulative plot on figure 3*B*.

We primarily used the THEMIS daytime IR mosaic to define the level of geologic mapping at 1:500,000 scale but used higher spatial and spectral resolution data to confirm contact boundaries and augment the Description of Map Units. These datasets include narrow-angle images from the MGS Mars Orbiter Camera (MOC, ~1.5–12 m/pixel resolution) (Malin and others, 2010), full resolution targets (FRT, ~ 20 m/pixel resolution) from the Compact Reconnaissance Imaging Spectrometer for Mars (CRISM) (Murchie and others, 2007) on MRO, and images from the High Resolution Imaging Science Experiment (HiRISE, ~0.25 m/pixel resolution) (McEwen and others, 2007) on MRO. We used ~50 HiRISE images (not including stereo images) to assess the 10-meter (m) to submeter morphology and sedimentary stratigraphy in and around Margaritifer basin and the lower reaches of Samara-Himera and Paraná-Loire Valles.

## Age Determinations

We used crater statistics and stratigraphic relations to assess the relative ages of surfaces. We compiled crater statistics in GIS software using a subset of a global CTX mosaic (Dickson and others, 2018), and CraterTools, a plug-in software for GIS (Kneissl and others, 2011). The resolution of the CTX mosaic, which covered nearly 100 percent of the map, enabled confident definition of craters >20 m in diameter and counts excluded obvious secondary clusters. To further reduce negative effects of varying image resolution and (or) gaps in coverage, we excluded craters with diameters <50 m from interpretation of ages. We derived the interpreted absolute ages for each count from segments of the plots for each unit that best match the expected production population using "pseudo-log" binned reverse cumulative histograms and Craterstats2 software (Michael and Neukum, 2010). We derived absolute ages based on the chronology function of Hartmann and Neukum (2001) and production function from Ivanov (2001). These tentative ages, based on the combined areas and counts for each unit (table 1; fig. 3), were consistent with observed superposition and crosscutting relations within the error bars of the crater counts. The geologic epoch associated with each count and range of epochs (table 1) covered by the error bars in figure 3 were based on the chronology function from Hartmann and Neukum (2001). Where unit areas were too small to provide meaningful ages from crater statistics (for example, vallis, mass wasting, and mountainous units, table 1), we incorporated characteristics of the same map units from adjacent maps (Grant and others, 2009; Irwin and Grant, 2013).

## Regional Geology

As summarized by Grant (1987) and Grant and Parker (2002), the Early Noachian features associated with the degraded Holden, Ladon, and Ares basin multi-ringed impact structures are the oldest features in Margaritifer Terra (fig. 1) (Schultz and Glicken, 1979; Schultz and others, 1982; Frey, 2008; Frey and others, 2001). The mapped region lies between the second and third rings of Ladon impact basin (fig. 1) (Schultz and Glicken, 1979; Schultz and others, 1982; Grant, 1987), and the center of the Ares multi-ringed impact basin is located to the north (Frey,

2008; Frey and others, 2001). Margaritifer Chaos is generally positioned between rings of the Ladon and Ares basins, although expression of the Ares basin rings is subtle (Schultz and others, 1982; Frey, 2008). The Holden and Ladon basins imparted considerable structural and topographic influence on the course of the ULM drainage, with incised segments turning as they cross the basin rims to become radial to depositional basin centers.

The relation between Margaritifer basin and the Chryse trough is uncertain. On the basis of the convergence of the ULM, Samara-Himera, and Paraná-Loire drainage networks into the basin, topographic expression of the Chryse trough predates the Late Noachian, partly because of its location near the trough axis (Grant and Parker, 2002). Unlike the nearby Ladon and Holden impact basins, Margaritifer basin is elongated (fig. 1) and the surrounding terrain does not preserve evidence of structural rings or other features that can be directly associated with an impact origin (Schultz and Glicken, 1979; Schultz and others, 1982; Frey and others, 2001); however, numerous occurrences of high-standing topography are visible within the basin. Additionally, Salvatore and others (2016) found no conclusive evidence supporting an impact origin for the basin in gravity data. More likely, Margaritifer basin represents a topographic low along the axis of the Chryse trough that was created and (or) bounded by remnant relief associated with the structural rings of Ladon basin (fig. 1).

The map area straddles the eastern expression of the Chryse trough, a linear topographic depression induced by loading of the lithosphere related to the Tharsis rise (Phillips and others, 2001) (fig. 1). The Chryse trough is hundreds of kilometers across and approximately 2 km deep in Margaritifer Terra and provides a first order pathway from drainage along the ULM system from Argyre basin (south of fig. 1 map area) to Margaritifer basin. Although a surface unit is not mapped in association with the Chryse trough, its structural control directly influenced the overall evolution and juxtaposition of units within the region. The circumferential compressional wrinkle ridges and radial graben throughout Margaritifer Terra were also caused by lithospheric loading related to the Tharsis rise (Grant, 1987). On the basis of valley orientations that are controlled by the trough, including the Samara-Himera and Paraná-Loire drainage networks, the topographic expression of the trough evolved in the Noachian and was largely complete by the Middle to Late Noachian (Phillips and others, 2001).

Formation of the multi-ringed impact basins and the Chryse trough was followed by evolution of the diverse cratered upland surface, shaped in part by multiple resurfacing events between the Early and Late Noachian and into the Hesperian Epochs. Some of these resurfacing events likely involved volcanic activity, whereas others are related to alluvial and (or) lacustrine deposition, and still others reflect the effects of multiple processes (for example, Irwin and Grant, 2013; Salvatore and others, 2016). The ULM outflow system and nearby valley networks incise most of these surfaces, but a final localized resurfacing event in the Hesperian emplaced materials that embay some valleys (Grant, 1987). Hence, major incision of the ULM system and valleys draining into Margaritifer basin occurred by the Late Noachian, but lesser flow may have persisted into the Hesperian (Grant, 1987; Irwin and Grant, 2009).

# Stratigraphy

## Noachian Period

The oldest map unit, mountainous unit (Nm), occurs as isolated bedrock promontories corresponding to exposure of deep crustal materials associated with the ancient, degraded rings of Ladon basin (Saunders, 1979; Schultz and others, 1982; Frey and others, 2001; Irwin and Grant, 2013). These mountains are at least Middle Noachian, ~3.7–3.9 billion years (Ga) (Irwin and Grant, 2013), and were reduced in size and extent by considerable degradation (lowering of surface as a result of erosion) that created fringing pediments or deposits of the terra unit.

One of the more extensive units in the region is the terra unit (HNt). In the vicinity of Margaritifer basin, the terra unit has thermal inertias of ~250 joules per square meter Kelvin root second ($J\ m^{-2}\ K^{-1}\ s^{-0.5}$) (Salvatore and others, 2016) that correspond to an effective grain size of ~230 micrometers (μm) (Presley and Christensen, 1997; Piqueux and Christensen, 2011). Although Salvatore and others (2016) noted that CRISM data of the terra unit in and around Margaritifer basin do not display spectrally diagnostic alteration features, modeled Thermal Emission Spectrometer (TES) mineralogy indicates unit HNt is dominated by plagioclase, pyroxene (dominantly low-calcium pyroxene), and amorphous and (or) alteration phases, which is typical of Noachian surfaces across the planet (Bibring and others, 2005; Rogers and Christensen, 2007). We derived crater densities of unit HNt that yield an estimated absolute age of 3.84 (±0.03) Ga, which indicates degradation of these surfaces occurred in the Late Noachian to Early Hesperian (fig. 3; table 1). This age is consistent with unit HNt surfaces mapped to the west by Irwin and Grant (2013).

As described by Irwin and Grant (2013), the terra unit incorporates a diverse assemblage of material that likely includes fractured basaltic bedrock (Bandfield and others, 2000), impact ejecta, weathered rocks (Murchie and others, 2009), fluvially reworked sediments, airfall or eolian traction materials, and perhaps other types of rocks. The terra unit occurs over a range of elevation and is composed of mostly sedimentary and (or) volcanic materials (Grant and Parker, 2002) that have undergone extensive modification by post-Noachian impact gardening (Hartmann and Neukum, 2001), eolian reworking, and fluvial dissection that precludes meaningful subdivision (Tanaka and others, 2005). As noted by Irwin and Grant (2013), terra unit surfaces are typically rolling and do not retain small craters well, relative to younger and smoother (at all length scales) basin fills. The terra unit consists of relatively competent materials that have troughs and occasional lobate margins and is locally streamlined by channel units in Margaritifer basin.

## Hesperian Period

Fluvial activity during multiple periods and at various scales greatly influenced the landscape within the map area. Preserved features indicate that regional, widespread channels and valley network formation within Margaritifer Terra occurred in the Late Noachian and extended into the Late Hesperian, but the possible destruction of older features means that earlier activity

cannot be ruled out. The preserved fluvial record is approximately coincident with widespread gradation elsewhere on Mars (Grant, 1987, 2000; Grant and Schultz, 1990, 1993).

The vallis unit (HNvn) includes the lowermost part of the trunk valleys of the Samara-Himera and Paraná-Loire drainage networks. The lowermost reaches of the well-incised Loire segment of Paraná-Loire Valles enter the map area from the southeast, but it quickly transitions to local collapsed terrain (chaotic 1 unit, $AHct_1$) that may be associated with ponding and infiltration of material upstream from a topographic high. Samara-Himera Valles emerges into the southern part of the map after coursing around the west side of Jones crater (fig. 1). The valley network drains across the Jones crater ejecta and takes on a degraded, but possibly braided, appearance (multiple bifurcations and apparent intervening bars) as it traverses northward into a shallow, 10 to 15-km-wide trough (fig. 4) defined by relief associated with rings of Ladon basin and along the axis of the Chryse trough (Grant and Parker, 2002). The valley is difficult to detect at CTX resolution within the trough before becoming incised as it exits to the north. The incised expression of the Samara part of the Samara-Himera valley system persists northward until it is buried by younger volcanic materials (unit AHv) near the south margin of Margaritifer basin. Nevertheless, it appears that the Samara-Himera and Paraná-Loire systems merge before entering Margaritifer basin (fig. 2), although overlying volcanic materials make this difficult to confirm.

The overall morphometry of valley networks and their associated basins indicates they were formed through limited runoff sourced by precipitation (Irwin and Grant, 2013) and precipitation-recharged groundwater sapping (Grant, 2000; Grant and Parker, 2002). The timing of valley formation within this region is concurrent with enhanced geomorphic activity elsewhere on Mars (for example, Grant and Schultz, 1990), indicating that valley formation was not caused by local endogenic processes. The vallis unit (HNvn) incises the terra unit (HNt), and some valleys are locally embayed by younger materials from the basin fill 2 unit ($HNb_2$) (fig. 5*A*). The relative timing of unit HNvn formation in the map area is therefore constrained by the interval between units HNt and $HNb_2$, which we interpret to correspond to an Early Hesperian (>3.6 Ga) to Late Noachian age (table 1).

Four craters along the east map boundary have flat floors infilled with basin fill 2 unit ($HNb_2$) materials that are disrupted by fractures and exhibit anomalously high thermal inertia in THEMIS nighttime IR data. The appearance of these craters is similar to craters to the west (Irwin and Grant, 2013) and southwest (McDowell and Hamilton, 2005) of the map area. The southernmost of these four craters has a floor sloping to the south and a central depression that extends to the northwest (fig. 5*C*), possibly along a fracture or zone of weakness. The occurrence of the central depression in the crater-fill material indicates it is not a primary signature of the impact process, similar to other central pits in some craters (Schultz, 1987). Fracturing and the central depression in this crater may indicate infill of lava from below followed by later draining of still-molten material (Wichman and Schultz, 1995). Molten material may have welled up into the crater then drained before it had fully solidified (perhaps in stages), leaving behind the terraced fractures, similar to other floor-fractured craters to the southwest (Irwin and Grant, 2013). Subsequent contraction because of cooling or draining of material could have created the fractures on the crater floors. Such an interpretation is consistent with the occurrence of several transverse ridges that may be related to lava flows (fig. 5*C*). Several small mounds on the floors of these craters could be kipukas of wall material, rootless cones, or mostly buried source vents (fig. 5*C*).

Morava Valles (channel units 1 [$HNch_1$] and 2 [$AHch_2$]) enter Margaritifer basin from the southwest and the channel bifurcates several times as it extends towards the northeast. The eroded morphology and widespread, presumably alluvial, surfaces in the channel distinguish it from the terra unit (Irwin and Grant, 2013). The floor of the channel units and margins of the channel are lightly to moderately cratered and appear rough at meter-scale and include polygonal fractures and networks of raised orthogonal ridges (Salvatore and others, 2016). As summarized by Salvatore and others (2016), the channel units display a variable albedo because of eolian mantling, THEMIS decorrelation stretch images are devoid of diagnostic characteristics, TES analyses are similar to unit HNt, and the average thermal inertia is 521±45 J $m^{-2}$ $K^{-1}$ $s^{-0.5}$. The thermal inertia equates to an effective mean grain size of greater than 1 millimeter (mm) but likely indicates a cemented regolith (Presley and Christensen, 1997; Piqueux and Christensen, 2011; Salvatore and others, 2016).

We used crosscutting relations, state of degradation, and crater densities to define at least two periods of fluvial dissection: the Late Noachian/Early Hesperian to Late Hesperian 3.54 (+0.08/−0.16) Ga channel 1 unit ($HNch_1$), and the Late Hesperian to Early Amazonian 2.64 (+0.27/−0.30) Ga channel 2 unit ($AHch_2$) (figs. 3*B*, 6; table 1). Channel 1 unit represents initial dissection of the terra surface; these channel surfaces were abandoned when subsequent flows coalesced and incised the channel 2 unit ($AHch_2$) (fig. 6). Although crude layering in Ladon basin indicates multiple pulses of discharge into Margaritifer basin (Grant and Parker, 2002), it is unclear how much time occurred between discharge events related to the dissection responsible for the present-day expression of Morava Valles. The surface of channel 2 unit exposes terraced bedrock outcrops, eroded surfaces of the terra unit, and veneers of alluvial sediment (fig. 7). The lack of deposits associated with unit $AHch_2$ (for example, embayment of basin fill units 2 and 3 within Margaritifer basin) indicates discharge associated with the formation of the channel 2 unit was limited and largely reworked surfaces of the channel 1 unit. Morava Valles terminate in collapse in the central part of Margaritifer basin, and the lack of evidence for fluid flow into or out of the collapse is consistent with collapse postdating the cessation of fluvial activity. The lack of an incised channel on the northeast margin of the chaos indicates that discharge from Morava Valles mostly ponded within Margaritifer basin.

The floor of Margaritifer basin was resurfaced by basin fill 1 unit ($HNb_1$) and basin fill 3 unit ($Hb_3$). Basin fill 1 unit occurs as patches of rough, scabby to knobby (at meters to hundreds of meters length scales), light-toned cratered material (fig. 8). As summarized by Salvatore and others (2016), unit $HNb_1$ corresponds to local outcrops mapped as a fractured unit that occurs at elevations >300 m, and some superposed craters sometimes contain layered fill. Basin fill 1 unit materials exhibit a distinct hydrated mineral signature in CRISM data that is consistent with the presence of a mixed Fe/Mg-smectite (Salvatore and others,

2016). The basin fill 1 material has a relatively high albedo and average thermal inertia of 374±26 J $m^{-2}$ $K^{-1}$ $s^{-0.5}$ (consistent with grain sizes >1 mm or cemented materials; Presley and Christensen, 1997; Piqueux and Christensen, 2011) relative to surrounding materials (Salvatore and others, 2016). Our mapping of unit $HNb_1$ used similar morphologic criteria described above but includes more widespread outcrops than identified by Salvatore and others (2016) via inclusion of some relatively darker surfaces that may possess a thin, dark-toned eolian mantle (fig. 8). The basin fill 1 unit underlies the basin fill 3 unit ($Hb_3$) and is exposed in places via erosion of the younger, smoother plains ($Hb_3$) (fig. 8). We propose an estimated absolute age for basin fill 1 unit of 3.62 (+0.04/−0.06) Ga from the crater statistics, which correlates to the Late Noachian/Early Hesperian boundary (fig. 3*B*; table 1).

The fine layering within unit $HNb_1$, occurrence of clays, and its fairly uniform and widespread occurrence across Margaritifer basin is consistent with deposition in a lacustrine setting (Grant and Parker, 2002) or large-scale alluvial environment (Salvatore and others, 2016). Although the relative importance of contributions to the deposit from Morava Valles versus Samara-Himera and Paraná-Loire Valles is uncertain, the distribution of unit $HNb_1$ in the basin may be consistent with sedimentation associated with early, larger-scale inundation of the basin related to discharge from the much larger Morava Valles. Hence, we interpret unit $HNb_1$ to be a depositional unit associated with early discharge from Morava Valles (unit $HNch_1$), consistent with the initial formation of the Samara-Himera and Morava Valles systems in the Late Noachian to Early Hesperian (Grant, 2000; Grant and Parker, 2002).

Basin fill 2 unit ($HNb_2$) is characterized by relatively smooth (kilometer-length scales), crater-retaining, darker toned surfaces with relatively high THEMIS nighttime IR temperatures (Irwin and Grant, 2013) and includes occasional wrinkle ridges and lobate margins. This unit occurs throughout the map area, most commonly in low-lying topography such as crater floors, yet is essentially absent within Margaritifer basin. The basin fill 2 unit embays the terra unit (fig. 5*B*) in MTM −15022 quadrangle and is modified by chaotic surfaces in MTM −10022 quadrangle. The crater densities we calculated yield an estimated absolute age of 3.63 (±0.02) Ga, implying emplacement in the Early to Late Hesperian (fig. 3*B*; table 1), consistent with unit $HNb_2$ surfaces to the west mapped by Irwin and Grant (2013). Based on these characteristics, we interpret unit $HNb_2$ as a moderately to strongly indurated unit of mostly volcanic material, with lesser indurated alluvial or eolian materials; origin and composition may vary within and between occurrences within individual basins (Irwin and Grant, 2013).

Basin fill 3 unit ($Hb_3$) within Margaritifer basin is younger than unit $HNb_1$ and is morphologically similar to unit $HNb_2$ in that both units are smooth and darker toned (figs. 7, 8). Salvatore and others (2016) mapped unit $Hb_3$ as a flat-lying plains unit and, although they distinguished two subunits, our map combines them at this scale. The basin fill 3 unit is crater retaining, but lightly cratered and smooth over kilometer-length scales (fig. 8). Surfaces are smooth to rougher at subkilometer spatial scales and often exhibit eolian bedforms or polygonal and hummocky fractures, respectively. The basin fill 3 unit embays unit HNt and is often bound by cliffs, with some occurrences along the margins of Margaritifer basin expressing fractures and graben. As summarized by Salvatore and others (2016), within Margaritifer basin, unit $Hb_3$ sometimes caps local mesas that reach ~100–200 m above the basin floor. Compression ridges occur within and around the unit and the sometimes-lobate margins embay preexisting terrain and display peripheral troughs (Leverington and Maxwell, 2004; Goudge and others, 2012). Salvatore and others (2016) noted a mean thermal inertia of 319±15 J $m^{-2}$ $K^{-1}$ $s^{-0.5}$ corresponding to surfaces composed of an effective grain size of coarse sand (Presley and Christensen, 1997; Piqueux and Christensen, 2011). TES linear-unmixing results indicate a basaltic composition with higher olivine abundances than unit HNt, and CRISM data show no evidence for hydrated or crystalline alteration phases (Salvatore and others, 2016).

Collectively, the composition and morphology of unit $Hb_3$ strongly indicate a volcanic origin, although the unit could also be a basaltic sedimentary cap (Salvatore and others, 2016). If volcanic, unit $Hb_3$ could be analogous to scoriaceous layers above the entablature and colonnade parts of the Columbia River Basalt (Long and Wood, 1986; Salvatore and others, 2016) and may be similar to other volcanic units identified throughout and nearby the ULM system (for example, Williams and others, 2005; Irwin and Grant, 2013). One possible source for units $HNb_2$ and $Hb_3$ are volcanic edifices (unit AHv) located along the south margin of Margaritifer basin near the mouth of Samara-Himera and Paraná-Loire Valles at lat −14° N., long 338° E. (Williams and others, 2005; Salvatore and others, 2016). We estimated the absolute age of unit $Hb_3$ using crater densities as 3.39 (+0.05/−0.08) Ga, implying emplacement in the Late Hesperian (fig. 3*B*; table 1). This absolute age is consistent with the stratigraphic relations with the channel units because unit $Hb_3$ embays unit $HNch_1$ and is crosscut by unit $AHch_2$.

Four conical, fan-shaped landforms (unit AHf) radiate from alcoves in two unnamed craters in the MTM −15022 quadrangle. Fan surfaces may contain raised ridges that radiate from the apex of the fan. Crater densities of unit AHf yield an estimated absolute age of 3.13 (+0.36/−2.10) Ga and an implied emplacement age ranging from the Late Hesperian to Middle Amazonian (fig. 3*A*; table 1). On the basis of their incised, fan-shaped morphology, we interpreted unit AHf as alluvial fans that are similar in morphology and age to fans to the southwest (Grant and Wilson, 2011, 2012; Irwin and Grant, 2013). We interpreted unit AHf as the youngest fluvial feature in the map area because it is emplaced on, and is therefore younger than, unit $HNb_2$.

The mass-wasting unit (AHmw) is located on the floor of an unnamed crater in MTM −15022 (lat −17.18° N., long 337.44° E.) and is an elongated, tongue-shaped deposit that lacks incised channels at the upper boundary. The unit is too small for meaningful crater statistics, but it is younger than the basin fill 2 unit ($HNb_2$) on which unit AHmw is superposed. The abrupt origin and downslope displacement of material indicates unit AHmw is the result of mass wasting, perhaps triggered by the formation of nearby impact craters.

## Amazonian Period

At least four partially collapsed mounds are located in the vicinity of one of the structural rings of Ladon basin (fig. 1) near the confluence of Samara-Himera and Paraná-Loire Valles (fig. 9). The mounds rise about a kilometer above the surrounding

plains (fig. 9*A*), and their flanks are composed of basaltic materials (Salvatore and others, 2016). We interpret these mounds to be volcanic in origin and map them as unit AHv (Williams and others, 2005; Salvatore and others, 2016). We estimate the absolute age of unit AHv as 2.84 (+0.34/−0.54) Ga, consistent with emplacement in the Early to Late Amazonian (fig. 3; table 1).

The elevated parts of the volcanic surfaces are characterized by small ridges that are concentric to the central region and occur at the highest points (fig. 9*B*). These ridges are not consistent with an eolian dune origin, and we interpret them to be sand waves produced by percussive shockwaves within the expanding cloud of a phreatomagmatic eruption (Dellino and others, 2004). Evidence for this type of volcanic landform has also been noted by Wilson and Head (2004) in Mangala Valles (outside of map area at lat −11.32 N., long 208.61 E.). The largest edifice on the margin of Margaritifer basin has two pits on its north flank that may be related to fluid that discharged from within its interior. These pits and possible flow could signify fluid discharge caused by ice melting because of magmatic heating. This heating could be related to an area of local chaotic terrain that emanates from the north contact of the edifice. The smaller edifices to the south of the largest edifice exhibit the dune-like features consistent with the interaction of hot material with ice and (or) water. One of these constructs disrupts the Loire segment of Paraná-Loire Valles and embays valleys to the south that likely emptied into the Loire segment, whereas the distal margin of the other feature obscures a part of Samara-Himera Valles.

The composition of the mounds (unit AHv) is consistent with that of unit $Hb_3$, which indicates that these putative volcanic edifices or earlier associated regional activity are related to, or caused by, unit $Hb_3$ (Salvatore and others, 2016). Moreover, the compositional similarity of unit $Hb_3$, the mounds, and volcanic materials identified elsewhere throughout the ULM system (Irwin and Grant, 2013) indicates they may share a common petrologic origin. Nevertheless, the contact between the unit AHv and units within Margaritifer basin is indistinct in some areas and the final activity associated with formation of the unit AHv mounds appears considerably younger, thereby making direct associations difficult. Possible association with one of the structural rings of Ladon basin could indicate a conduit for much later extrusion of the material forming the mounds.

## Structural Features

Areas of collapse, known as Margaritifer Chaos, dominate the northwest and northeast corners of the map and are divided into two types on the basis of local relief and degree of surface disruption. We identify chaotic 1 unit ($AHct_1$) by collapse pits, structurally controlled lineaments, and local patches of knobby terrain and (or) elevated knobs and plateaus of material that have been broken up by collapse. These surfaces exhibit structural disruption that is typically <500 m lower than the surrounding terrain and >50 percent of the original surface remains intact. We characterize chaotic 2 unit ($AHct_2$) as surfaces with severe structural disruption, resulting in irregular patches of closely spaced knobs or irregular blocks of similar heights within depressions that are typically >500 m deep relative to the surrounding terrain, and <50 percent of the original surface remains intact. The chaotic units ($AHct_1$ and $AHct_2$) are interpreted to reflect different magnitudes of collapse caused by differences in the amount of subsurface material removed as they formed. From crater densities, we estimate the absolute ages of units $AHct_1$ and $AHct_2$ as 1.38 (±0.20) Ga and 1.03 (±0.27) Ga, respectively, implying an Early to Middle Amazonian age, although collapse may have started in the Late Hesperian (fig. 3*A*; table 1). Mapping relations show that collapse is not modified by any of the other units and is one of the youngest units in the map area.

These chaotic surfaces occur in some areas of units HNt and $HNb_2$ but are prevalent within Margaritifer basin, where water may have infiltrated into the subsurface at lower elevations and collapse may have been caused by melting or sublimation of near-surface ice (Carr, 1979; Grant and Parker, 2002). Most of the chaotic units lie between the mapped location of structural rings associated with Ladon basin and may relate to inherent structural weakness imparted by formation of the basin (for example, Schultz and Glicken, 1979; Schultz and others, 1982).

## Geologic Summary

The geomorphologic evolution of the landscape in MTM −10022 and −15022 quadrangles records a long and complex history of resurfacing and modification by flowing water (for example, Rotto and Tanaka, 1995; Grant and Parker, 2002; Irwin and Grant, 2013; Salvatore and others, 2016). Active processes included volcanic and valley-forming processes that left a record that is among the best preserved on Mars (Grant, 2000). The resultant geologic history is generally similar to the broad-scale evolution established for quadrangles mapped at similar scale to the southeast (Grant and others, 2009) and southwest (Irwin and Grant, 2013).

The broad-scale topography and surface relief of the map region was shaped during the Noachian by the formation of the Holden and Ladon basins (Saunders, 1979; Schultz and Glicken, 1979; Schultz and others, 1982; Frey and others, 2001; Irwin and Grant, 2013) and the Chryse trough (Phillips and others, 2001) (fig. 1). The basins and broad-scale northward-converging drainage established by these early events controlled the location of most subsequent events in the region. Isolated mountains related to Ladon basin persist in the map area, and the juxtaposition of relief associated with the ancient basin rings and the Chryse trough created the topographic low that is Margaritifer basin.

Multiple processes modified the ancient surface until the Late Noachian and resulted in the formation of the terra unit that forms the widely exposed surface. Later resurfacing associated with likely sedimentary and volcanic processes then modified predominantly lower elevation surfaces and basins during the Late Noachian through at least the Hesperian.

Sedimentary processes during the Late Noachian were dominated by fluvial incision of the Samara-Himera and Paraná-Loire valley networks and the more voluminous discharge related to dissection of Morava Valles. Samara-Himera Valles clearly incise, and are younger than, the terra unit and

also appear to incise ejecta from Jones crater, which is located just south of the map area (fig. 1). The valley walls and floor maintain a fairly crisp morphology along much of its traverse through the map area, with several likely preserved longitudinal bars (fig. 4). Within parts of the trough near the south margin of the map, however, the diffuse expression of the valley results in a less obvious relation with bounding units. Nevertheless, the increased width through this section implies that the system became braided and (or) was characterized by local deposition within the trough and that the resultant subdued form has since been modified by eolian degradation relative to more incised segments to the north.

Geomorphic activity within Margaritifer basin was more complex and was likely dominated by the evolution of Morava Valles relative to the valley network formation. Within Margaritifer basin, elevated blocks of unit HNt are surrounded by likely lacustrine plains associated with unit $HNb_1$ and related to sedimentation in water ponded during early discharge from Morava Valles. These probable lacustrine plains are embayed by volcanic plains material (unit $Hb_3$). Although early drainage into the basin likely began during the Noachian (Irwin and Grant, 2013), the younger unit $Hb_3$ is as old as the Hesperian. Crater densities distinguish the ages of units within Margaritifer basin and, combined with cross-cutting relations, point to basin evolution over a relatively short period of geologic time. Both units $HNch_1$ and $HNb_1$ are stratigraphically above the terra unit and below unit $Hb_3$. The timing of the last drainage out of Morava Valles is not well constrained but could have occurred during the Hesperian on the basis of the timing of late activity in upstream segments of the ULM system (Grant and Parker, 2002; Grant and others, 2010; Irwin and Grant, 2013).

Collapse and resultant formation of chaotic terrain concentrated in the north part of the map area resulted in Margaritifer Chaos and other chaotic terrains that make it difficult to assess whether drainage along the ULM outflow system was continuous through Margaritifer basin and into Ares Vallis (Rotto and Tanaka, 1995; Grant and Parker, 2002) and (or) Mawrth Vallis (Irwin and Grant, 2009) systems to the north. Given the scale of the ULM outflow system and associated features mapped herein and to the southwest (Irwin and Grant, 2013), and the paucity of landforms comparable to units $NHch_1$ or $AHch_2$ beyond the middle part of Margaritifer basin and units equivalent to $HNb_1$ in the vicinity of Margaritifer Chaos, continuous flow into the drainages farther to the north (Rotto and Tanaka, 1995) appears less likely. Moreover, the occurrence of unit $HNb_1$ of likely lacustrine origin and the younger chaotic terrain within and around the periphery of Margaritifer basin is more consistent with drainage into the basin and associated flooding, followed by infiltration and storage in the subsurface before later release during formation of the chaotic terrain (Grant and Parker, 2002).

The trigger for collapse leading to formation of the chaotic terrain (units $AHct_1$ and $AHct_2$) may have been related to late volcanic activity associated with volcanic constructs (AHv) along the south margin of Margaritifer basin (fig. 9). We interpret the volcanic rocks to be the result of at least localized magmatic activity that could have taken advantage of zones of weakness along one of the outer rings of the Ladon impact basin. Consequently, magmatic activity associated with ancient basin structure may be expected elsewhere in the region and indicates that emplacement of units $HNb_2$ or $Hb_3$ may have been contemporaneous. Associated local subsurface heating may be responsible for collapse terrain that resulted from removal of subsurface material, likely frozen water that infiltrated into the subsurface during ponding within the ULM outflow system. This regional activity could have led to melting of water stored as ice in the subsurface, thereby leading to collapse, discharge, and the contribution to source of water that carved Ares and (or) Mawrth Valles (Rotto and Tanaka, 1995; Grant and Parker, 2002; Irwin and Grant, 2009).

The final geomorphic events in the map area included activity during the late Hesperian and perhaps into the Amazonian that formed local alluvial fans within some craters (for example, Grant and Wilson, 2011, 2012; Irwin and Grant, 2013) and isolated mass wasting on steep slopes that likely continues sporadically today. A final, variable veneer associated with locally occurring impacts and redistribution of fine-grained material by the wind resulted in the landscape observed today.

## Acknowledgements

This work was sponsored by NASA Planetary Geology and Geophysics Program grants NAG5-4157 and NAG5-10390. The authors thank Corey Fortezzo of the USGS for assistance with GIS mapping techniques, and the Map Coordinator, Jim Skinner, for his guidance. This map and associated documents were improved by comments from several anonymous reviewers.

## References Cited

Baker, V.R., 1982, The channels of Mars: Austin, University of Texas Press, 198 p.

Baker, V.R., Carr, M.H., Gulick, V.C., Williams, C.R., and Marley, M.S., 1992, Channels and valley networks, *in* Kieffer, H.H., Jakosky, B.M., Snyder, C.W. and Matthews, M.S., eds., Mars: Tucson, Ariz., University of Arizona Press, p. 493–522.

Baker, V.R. and Nummedal, D., eds., 1978, The Channeled Scabland: Washington, D.C., National Aeronautics and Space Administration, Planetary Geology Program, 186 p.

Bandfield, J.L., Hamilton, V.E., and Christensen, P.R., 2000, A global view of Martian surface compositions from MGS-TES: Science, v. 287, p. 1626–1630, https://doi.org/10.1126/science.287.5458.1626.

Bibring, J.-P., Langevin, Y., Gendrin, A., Gondet, B., Poulet, F., Berthé, M., Soufflot, A., Arvidson, R., Mangold, N., Mustard, J., Drossart, P., and the OMEGA Team, 2005, Mars surface diversity as revealed by the OMEGA/Mars Express observations: Science, v. 307, p. 1576–1581, https://doi.org/10.1126/science.1108806.

Boothroyd, J.C., 1982, Ancient fluvial drainage systems—Margaritifer Sinus area, Mars, *in* Reports of planetary

geology program—1982: Washington, D.C., National Aeronautics and Space Administration Technical Memorandum 85127, p. 209–212.
Carr, M.H., 1979, Formation of Martian flood features by the release of water from confined aquifers: Journal of Geophysical Research, v. 84, p. 2995–3007.
Carr, M.H., 1981, The surface of Mars: New Haven, Conn., Yale University Press, 232 p.
Carr, M.H., 1996, Water on Mars: New York, Oxford University Press, 229 p.
Carr, M.H., 2006, The surface of Mars: Cambridge, U.K., Cambridge Planetary Science Series, Cambridge University Press.
Christensen, P.R., Jakosky, B.M., Kieffer, H.H., Malin, M.C., McSween, H.Y., Jr., Nealson, K., Mehall, G.L., Silverman, S.H., Ferry, S., Caplinger, M., and Ravine, M., 2004, The Thermal Emission Imaging System (THEMIS) for the Mars 2001 Odyssey Mission: Space Science Reviews, v. 110, 85–130.
Dellino, P., Isaia, R., La Volpe, L. and Orsi, G., 2004, Interaction between particles transported by fallout and surge in the deposits of the Agnano-Monte Spina eruption (Campi Flegrei, southern Italy): Journal of Volcanology and Geothermal Research, v. 133, p. 193–210.
Dickson, J.L., Kerber, L.A., Fassett, C.I, and Ehlmann, B.L., 2018, A global, blended CTX mosaic of Mars with vectorized seam mapping—A new mosaicking pipeline using principles of non-destructive image editing [abs.]: Lunar and Planetary Science Conference, 49th, March 19–23, 2018, no. 2480.
Fassett, C.I., and Head, J.W., III, 2008, Valley network-fed, open-basin lakes on Mars—Distribution and implications for Noachian surface and subsurface hydrology: Icarus, v. 198, p. 37–56, https://doi.org/10.1016/j.icarus.2008.06.016.
Ford, J.P., Plaut, J.J, Weitz, C.M., Farr, T.G., Senske, D.A., Stofan, E.R., Michaels, G., and Parker, T.J., 1993, Guide to Magellan image interpretation: Washington, D.C., National Aeronautics and Space Administration, Jet Propulsion Laboratory Publication 93-24.
Frey, H.V., 2008, Ages of very large impact basins on Mars—Implications for the late heavy bombardment in the inner solar system: Geophysical Research Letters, v. 35, https://doi.org/10.1029/2008GL033515.
Frey, H.V., Frey, E.L., Sakimoto, S.E.H., Shockey, K., and Roark, J., 2001, A very large population of likely buried impact basins in the northern lowlands of Mars revealed by MOLA data: Lunar and Planetary Science Conference, 32d, March 12–16, 2001, no. 1680.
Goudge, T.A., Head, J.W., III, Mustard, J.F., and Fassett, C.I., 2012, An analysis of open basin lake deposits on Mars—Evidence for the nature of associated lacustrine deposits and post-lacustrine modification processes: Icarus, v. 219, p. 211–229, https://doi.org/10.1016/j.icarus.2012.02.027.
Grant, J.A., 1987, The geomorphic evolution of eastern Margaritifer Sinus, Mars, *in* Advances in Planetary Geology: Washington, D.C., National Aeronautics and Space Administration Technical Memorandum 89871, p. 1–268.
Grant, J.A., 2000, Valley formation in Margaritifer Sinus, Mars, by precipitation-recharged ground-water sapping: Geology, v. 28, p. 223–226.
Grant, J.A., Irwin, R.P., III, Tanaka, K.L., Skinner, Jr., J.A, and Hare, T.M., 2011, Planetary geologic mapping handbook—2011: U.S. Geological Survey, Astrogeology Science Center, unpublished handbook Grotzinger, J.P., Milliken, R.E., Tornabene, L.L. McEwen, A.S., Weitz, C.M., Squyres, S.W., Glotch, T.D., and Thomson, B.J., 2008, HiRISE imaging of impact megabreccia and sub-meter aqueous strata in Holden Crater, Mars: Geology, v. 36, p. 195–198, https://doi.org/10.1130/G24340A.
Grant, J.A., Irwin, R.P., III, Wilson, S.A., Buczkowski, D., and Siebach, K., 2010, A lake in Uzboi Vallis and implications for late Noachian-Early Hesperian climate on Mars: Icarus, v. 212, p. 110–122, https://doi.org/10.1016/j.icarus.2010.11.024.
Grant, J.A., and Parker, T.J., 2002, Drainage evolution of the Margaritifer Sinus region, Mars: Journal of Geophysical Research, v. 107, 19 p., https://doi.org/10.1029/2001JE001678.
Grant, J.A., and Schultz, P.H., 1990, Gradational epochs on Mars—Evidence from west-northwest of Isidis basin and Electris: Icarus, v. 84, p. 166–195.
Grant, J.A., and Schultz, P.H., 1993, Degradation of selected terrestrial and Martian impact craters: Journal of Geophysical Research, v. 98, p. 11,025–11,042.
Grant, J.A., and Wilson, S.A., 2011, Late alluvial fan formation in southern Margaritifer Terra, Mars: Geophysical Research Letters, v. 38, 6 p., https://doi.org/10.1029/2011GL046844.
Grant, J.A., and Wilson, S.A., 2012, A possible synoptic source of water for alluvial fan formation in southern Margaritifer Terra, Mars: Planetary Space Science, v. 72, p. 44–52, https://doi.org/10.1016/j.pss.2012.05.020.
Grant, J.A., Wilson, S.A., Fortezzo, C.M., and Clark, D.A., 2009, Geologic map of MTM −20012 and −25012 quadrangles, Margaritifer Terra region of Mars: U.S. Geological Survey Scientific Investigations Map 3041, scale 1:500,000, https://pubs.usgs.gov/sim/3041/.
Greeley, R., and Batson, R., eds., 1990, Planetary mapping: Cambridge, U.K., Cambridge University Press, 296 p.
Greeley, R., and Guest, J.E., 1987, Geologic map of the eastern equatorial region of Mars, U.S. Geological Survey Scientific Investigations Map I–1802–B, scale 1:15,000,000.
Hartmann, W.K., and Neukum, G., 2001, Cratering chronology and the evolution of Mars: Space Science Reviews, v. 96, p. 165–194.
Howard, A.D., Moore, J.M., and Irwin, R.P., III, 2005, An intense terminal epoch of widespread fluvial activity on early Mars—1. Valley network incision and associated deposits: Journal of Geophysical Research, v. 110, 20 p., https://doi.org/10.1029/2005JE002459.
Ivanov, B.A., 2001, Mars/Moon cratering ratio estimates: Space Science Review, v. 96, p. 87–104.
Irwin, R.P., III, Grant, J.A., 2009, Large basin overflow floods on Mars, *in* Burr, D.M., Baker, V.R., and Carling, P.A., eds., Megaflooding on Earth and Mars: Cambridge, U.K., Cambridge University Press, p. 209–224.
Irwin, R.P., III, Grant, J.A., 2013, Geologic map of MTM −15027, −20027, −25027, and −25032 quadrangles, Margaritifer Terra region of Mars: U.S. Geological Survey Scientific Investigations Map 3209, scale 1:1,000,000, https://doi.org/10.3133/sim3209.

Komar, P.D., 1979, Comparisons of the hydraulics of water flows in Martian outflow channels with flows of similar scale on earth: Icarus, v. 37, no. 1, p. 156–181, https://doi.org/10.1016/0019-1035(79)90123-4.

Kneissl, T., van Gasselt, S., and Neukum, G., 2011, Map-projection-independent crater size-frequency determination in GIS environments—New software tool for ArcGIS: Planetary and Space Science, v. 59, p. 1243–1254, https://doi.org/10.1016/j.pss.2010.03.015.

Leverington, D.W., and Maxwell, T.A., 2004, An igneous origin for features of a candidate crater-lake system in western Memnonia—Mars: Journal of Geophysical Research, v. 109, https://doi.org/10.1029/2004JE002237.

Long, P.E., and Wood, B.J., 1986, Structures, textures, and cooling histories of Columbia River basalt flows: Geological Society of America Bulletin, v. 97, p. 1144–1155.

Malin, M.C., Bell, J.F., III, Cantor, B.A., Caplinger, M.A., Calvin, W.M., Clancy, R.T., Edgett, K.S., Edwards, L., Haberle, R.M., James, P.B., Lee, S.W., Ravine, M.A., Thomas, P.C., Wolff, M.J., 2007, Context Camera investigation on board the Mars Reconnaissance Orbiter: Journal of Geophysical Research, v. 112, , https://doi.org/10.1029/2006JE002808.

Malin, M.C., Edgett, K.S., Cantor, B.A., Caplinger, M.A., Danielson, G.E., Jensen, E.H., Ravine, M.A., Sandoval, J.L., and Supulver, K.D., 2010, An overview of the 1985–2006 Mars Orbiter Camera science investigation: Mars, v. 5, p. 1–60, https://doi.org/10.1555/mars.2010.0001.

Mars Channel Working Group, 1983, Channels and valleys on Mars: Geological Society of America Bulletin, v. 94, p. 1035–1054.

McDowell, M.L., and Hamilton, V.E., 2005, Characteristics of intracrater thermal anomalies in southwestern Margaritifer Terra [abs.]: Lunar and Planetary Science Conference, 36th, March 14–18, 2005, no. 1548.

McEwen, A.S., Eliason, E.M., Bergstrom, J.W., Bridges, N.T., Hansen, C.J., Delamere, W.A., Grant, J.A., Gulick, V.C., Herkenhoff, K.E., Keszthelyi, L., Kirk, R.L., Mellon, M.T., Squyres, S.W., Thomas, N., Weitz, C.M., 2007, Mars Reconnaissance Orbiter's High Resolution Imaging Science Experiment (HiRISE): Journal of Geophysical Research, v. 112, 40 p., https://doi.org/10.1029/2005JE002605.

Melosh, J. M., 1989, Impact cratering—A geologic process: New York, Oxford University Press, 245 p.

Michael, G.G., and Neukum, G., 2010, Planetary surface dating from crater size-frequency distribution measurements—Partial resurfacing events and statistical age uncertainty: Earth and Planetary Science Letters, v. 294, p. 223–229, https://doi.org/10.1016/j.epsl.2009.12.041.

Mutch, T.A., Arvidson, R.E., Head, J.W., III, Jones, K.L. and Saunders, R.S., 1976, The geology of Mars: Princeton, N.J., Princeton University Press, 400 p.

Murchie, S., Arvidson, R., Bedini, P. Beisser, K., Bibring, J.-P., Bishop, J., Boldt, J., Cavender, P., Choo, T., Clancy, R.T., Darlington, E.H., Des Marais, D., Espiritu, R., Fort, D., Green, R., Guinness, E., Hayes, J., Hash, C., Heffernan, K., Hemmler, J., Heyler, G., Humm, D., Hutcheson, J., Izenberg, N., Lee, R., Lees, J., Lohr, D., Malaret, E., Martin, T., McGovern, J.A., McGuire, P., Morris, R., Mustard, J., Pelkey, S., Rhodes, E., Robinson, M., Roush, T., Schaefer, E., Seagrave, G., Seelos, F., Silverglate, P., Slavney, S., Smith, M., Shyong, W.-J., Strohbehn, K., Taylor, H., Thompson, P., Tossman, B., Wirzburger, M., and Wolff, M., 2007, Compact Reconnaissance Imaging Spectrometer for Mars (CRISM) on Mars Reconnaissance Orbiter (MRO): Journal of Geophysical Research, v. 112, 57 p., https://doi.org/10.1029/2006JE002682.

Murchie, S.L., Mustard, J.F., Ehlmann, B.L., Milliken, R.E., Bishop, J.L., McKeown, N.K., Noe Dobrea, E.Z., Seelos, F.P., Buczkowski, D.L., Wiseman, S.M., Arvidson, R.E., Wray, J.J., Swayze, G., Clark, R.N., Des Marais, D.J., McEwen, A.S., and Bibring J.-P., 2009, A synthesis of Martian aqueous mineralogy after 1 Mars year of observations from the Mars Reconnaissance Orbiter: Journal of Geophysical Research, v. 114, article E00D06, 30 p., https://doi.org/10.1029/2009JE003342.

Parker, T.J., 1985, Geomorphology and Geology of the Southwestern Margaritifer Sinus-Northern Argyre Region of Mars: Los Angeles, California State University, Los Angeles, M.S. thesis.

Parker, T.J., 1994, Martian paleolakes and oceans: Los Angeles, University of Southern California, Ph.D. dissertation.

Phillips, R.J., Zuber, M.T., Solomon, S.C., Golombek, M.P., Jakosky, B.M., Banerdt, W.B., Smith, D.E., Williams, R.M.E., Hynek, B.M., Aharonson, O., and Hauck II, S.A., 2001, Ancient geodynamics and global-scale hydrology on Mars: Science, v. 291, p, 2587–2591.

Piqueux, S., and Christensen, P.R., 2011, Temperature-dependent thermal inertia of homogeneous Martian regolith: Journal of Geophysical Research, v. 116, 18 p., https://doi.org/10.1029/2011JE003805.

Pondrelli, M., Baliva, A., Di Lorenzo, S., Marinangeli, L., and Rossi, A.P., 2005, Complex evolution of paleolacustrine systems on Mars—An example from the Holden crater: Journal of Geophysical Research, v. 110, 20 p., https://doi.org/10.1029/2004JE002335.

Presley, M.A., and Christensen, P.R., 1997, Thermal conductivity measurements of particulate materials, part I—A review: Journal of Geophysical Research v. 102, p. 6535–6549.

Rogers, A.D., and Christensen, P.R., 2007, Surface mineralogy of Martian low-albedo regions from MGS-TES data—Implications for upper crustal evolution and surface alteration: Journal of Geophysical Research, v. 112, https://doi.org/10.1029/2006JE002727.

Rotto, S., and Tanaka, K.L., 1995, Geologic/geomorphic map of the Chryse Planitia region of Mars: U.S. Geological Survey Miscellaneous Investigations Series Map I–2441, scale 1:5,000,000.

Salvatore, M.R., Kraft, M.D., Edwards, C.S., and Christensen, P.R., 2016, The geologic history of Margaritifer Basin: Journal of Geophysical Research, v. 121, 23 p., https://doi.org/10.1002/2015JE004938.

Saunders, S.R., 1979, Geologic map of the Margaritifer Sinus quadrangle of Mars: U.S. Geological Survey Mars Map Series I–1144, quadrangle MC-19, scale 1:5,000,000.

Schultz, P.H., 1987, Impact velocity and changes in crater shape, morphology, and statistics [abs.]: Lunar and Planetary Science Conference, 18th, March 16–20, 1987, no. 1453, p. 886–887.

Schultz, P.H., and Glicken, H., 1979, Impact crater and basin control of igneous processes on Mars: Journal of Geophysical Research, v. 84, p. 8033–8047.

Schultz, P.H., Schultz, R.A. and Rogers, J., 1982, The structure and evolution of ancient impact basins on Mars: Journal of Geophysical Research, v. 87, p. 9803–9820.

Scott, D.H. and Tanaka, K.L., 1986, Geologic map of the western equatorial region of Mars: U.S. Geological Survey Miscellaneous Investigation Series Map I-1802-A, scale 1:15,000,000.

Skinner, J.A., Jr., Huff, A.E., Fortezzo, C.M., Gaither, T.A., Hare, T.M., and Hunter, M.A., 2018, Planetary geologic mapping protocol—2018: Flagstaff, Ariz. The Planetary Geologic Map Coordination Group, U.S. Geological Survey Astrogeology Science Center, 33 p. [Also available online at https://astropedia.astrogeology.usgs.gov/download/Docs/Mappers/PGM_Protocol_March_2018.pdf.]

Smith, D.E., Zuber, M.T., Frey, H.V., Garvin, J.B., Head, J.W., Muhleman, D.O., Pettengill, G.H., Phillips, R.J., Solomon, S.C., Zwally, H.J., Banerdt, W.B., Duxbury, T.C. Golombek, M.P., Lemoine, F.G., Neumann, G.A., Rowlands, D.D., Aharonson, O., Ford, P.G., Ivanov, A.B., McGovern, P.J., Abshire, J.B., Afzal, R.S., and Sun, X., 2001, Mars Orbiter Laser Altimeter (MOLA)—Experiment summary after the first year of global mapping of Mars: Journal of Geophysical Research, v 106, p. 23,689–23,722.

Tanaka, K.L., Moore, H.J., Schaber, G.G., Chapman, M.G., Stofan, E.R., Campbell, D.B., Davis, P.A, Guest, J.E., McGill, G.E., Rogers, P.G., Saunders, R.S., and Zimbelman, J.R., 1994, The Venus geologic mappers' handbook: U.S. Geological Survey Open-File Report 94–438, 66 p.

Tanaka, K., Skinner, J.A., Jr., Dohm, J.M., Irwin, R.P., III, Kolb, E.J., Fortezzo, C.M., Platz, T., Michael, G.G., and Hare, T.M., 2014, Geologic map of Mars: U.S. Geological Survey Scientific Investigations Map 3292, scale 1:20,000,000, pamphlet 43 p.

Tanaka, K.L., Skinner, J.A., Jr., and Hare, T.M, 2005, Geologic map of the northern plains of Mars: U.S. Geological Survey Scientific Investigations Map 2888, scale 1:15,000,000.

Tanaka, K.L., Skinner, J.A., Jr., and Hare, T.M., 2011, Planetary geologic mapping handbook—2011: U.S. Geological Survey, Astrogeology Science Center, unpublished handbook, accessed March 4, 2021, at https://astropedia.astrogeology.usgs.gov/download/Docs/Mappers/PGM_Handbook_2011.pdf.

Wichman, R.W., and Schultz, P.H., 1995, Floor-fractured craters in Mare Smythii and west of Oceanus Procellarum—Implications of crater modification by viscous relaxation and igneous intrusion models: Journal of Geophysical Research, v. 100, p. 21,201–21,218.

Williams, K.K., Grant, J.A., and Fortezzo, C.M., 2005, New insights into the geologic history of Margaritifer Sinus and discovery of a phreatomagmatic event during late stage fluvial activity [abs.]: Lunar and Planetary Science Conference, 36th, March 14–18, 2005, no. 1439.

Wilson, L., and Head, J.W., III, 2004, Evidence for a massive phreatomagmatic eruption in the initial stages of formation of the Mangala Valles outflow channel, Mars: Journal of Geophysical Research, v. 31, 4 p., https://doi.org/10.1029/2004GL020322.

Wilson, S.A., Grant, J.A., Howard, A.D., and Buczkowski, D.L., 2018, The nature and origin of deposits in Uzboi Vallis on Mars: Journal of Geophysical Research, Planets, v. 123, p. 1842–1862, https://doi.org/10.1029/2017JE005508.